Journal of
Synchrotron Radiation
ISSN 0909-0495
Editors: **Å. Kvick, D. M. Mills and T. Ohta**

Multilayer X-ray optics at CHESS

Alexander Kazimirov, Detlef-M. Smilgies, Qun Shen, Xianghui Xiao, Quan Hao, Ernest Fontes, Donald H. Bilderback, Sol M. Gruner, Yuriy Platonov and Vladimir V. Martynov

Journal of
Synchrotron Radiation
ISSN 0909-0495

Received 13 December 2005
Accepted 23 January 2006

Multilayer X-ray optics at CHESS

Alexander Kazimirov,[a]* Detlef-M. Smilgies,[a] Qun Shen,[a] Xianghui Xiao,[a] Quan Hao,[a] Ernest Fontes,[a] Donald H. Bilderback,[a] Sol M. Gruner,[a] Yuriy Platonov[b] and Vladimir V. Martynov[b]

[a]Cornell High Energy Synchrotron Source (CHESS), Cornell University, Ithaca, NY 14853-8001, USA, and [b]Osmic Inc., 1900 Taylor Road, Auburn Hills, MI 48326, USA. E-mail: ayk7@cornell.edu

Almost half of the X-ray beamlines at the Cornell High Energy Synchrotron Source (CHESS) are based on multilayer optics. 'Traditional' multilayers with an energy resolution of $\Delta E/E \simeq 2\%$ are routinely used to deliver X-ray flux enhanced by a factor of 10^2 in comparison with standard Si(111) optics. Sagittal-focusing multilayers with fixed radius provide an additional factor of 10 gain in flux density. High-resolution multilayer optics with $\Delta E/E \simeq 0.2\%$ are now routinely used by MacCHESS crystallographers. New wide-bandpass multilayers with $\Delta E/E = 5\%$ and 10% have been designed and tested for potential applications in macromolecular crystallography. Small d-spacing multilayers with $d \leq 20$ Å have been successfully used to extend the energy range of multilayer optics. Analysis of the main characteristics of the Mo/B_4C and W/B_4C small d-spacing multilayer optics shows enhancement in their performance at higher energies. Chemical vapour deposited SiC, with a bulk thermal conductivity of a factor of two higher than that of silicon, has been successfully introduced as a substrate material for multilayer optics. Characteristics of different types of multilayer optics at CHESS beamlines and their applications in a variety of scattering, diffraction and imaging techniques are discussed.

Keywords: X-ray optics; multilayers; energy resolution.

1. Introduction

Shortly after the first 'layered synthetic microstructures', nowadays commonly known as multilayers (MLs), had been successfully produced and tested as Bragg diffracted optical elements for soft X-rays and EUV radiation (Haelbach & Kunz, 1976; Barbee, 1981; Underwood & Barbee, 1981), feasibility studies began at CHESS to design ML-based monochromators for hard X-ray synchrotron radiation (Bilderback, 1982; Bilderback *et al.*, 1983). In the 1990s, owing to remarkable progress in polishing technology, silicon substrates with surface figure errors within 2 Å RMS roughness and 1 arcsec slope error became available for ML coating.[1] Significant efforts have been launched at the synchrotron radiation laboratories around the world to introduce ML optics into synchrotron-radiation-based experiments at the second-generation (Underwood *et al.*, 1988; Stephenson, 1988; Pennartz *et al.*, 1992; Ziegler *et al.*, 1992) and, later, at the third-generation synchrotron radiation sources (*e.g.* Deschamps *et al.*, 1995; Chu *et al.*, 2002). In 1995, CHESS users performed their first experiments with beams produced by ML optics and, in 1997, a double-ML monochromator was permanently installed at the D1 bending-magnet beamline primarily for the purposes of small-angle scattering and fluorescence analysis. Since then, increasing the X-ray flux by designing and testing new ML optics has been among the highest priorities of the CHESS X-ray optics group. The main efforts have concentrated on the design of internally water-cooled MLs and sagittally focusing MLs for wiggler beamlines (Smolenski *et al.*, 1997, 1998, 2001; Headrick *et al.*, 2002).

During the last few years, the CHESS ML optics have been significantly upgraded. The growth of the number of CHESS 'multilayer' beamlines is based on advances in ML technology that resulted in the development of new optics with unique characteristics. A large variety of new MLs have been tested at CHESS, providing valuable feedback for further optimization of the ML technology and determining target parameters for the final optics optimized for their use in specific synchrotron radiation experiments. The goal of this article is to present the most recent update of these new developments. In the next sections, after a brief description of the 'multilayer' CHESS beamlines, we will report on high-resolution MLs with $\Delta E/E \simeq 0.2\%$ (§3), new wide-bandpass optics (§4), small d-spacing MLs and their main characteristics in the energy range from 14 keV to 60 keV (§5), optics for wiggler beamlines including

[1] Substrates for ML optics described in this article have been polished by Wave Precision (formerly General Optics).

Table 1
CHESS beamlines employing multilayer optics.

W: wiggler; BM: bending magnet; e^-: electrons; e^+: positrons. Listed here are the ML optics permanently assigned to these beamlines (a variety of other ML optics can be used at most of these beamlines for feasibility experiments). Usage refers to the fraction of time ML optics are used on the station; y = yes, n = no.

Beamline	Source	Sagittal focusing	Usage	*d*-spacing, materials	$\Delta E/E$ (%)	Experimental techniques/application areas
A2	W, e^-	y	50%	15 Å, Mo/B_4C	0.3	*In situ* diffraction/scattering
				20 Å, Mo/B_4C	0.6	Radiography
				28 Å, W/B_4C	1.9	Microbeam fluorescence
						Microbeam diffraction
D1	BM, e^+	n	100%	15 Å, W/B_4C	0.55	Small- and wide-angle scattering
				25 Å, W/C	1.7	Fluorescence imaging
				30 Å, Mo/B_4C	1.4	Radiography
F3	BM, e^+	n	50%	27 Å, W/C	2.2	Macromolecular crystallography
				24 Å, W/B_4C	0.8	Radiation damage in protein crystals
				22 Å, Mo/B_4C	0.7	
G1	W, e^+	y	100%	24 Å, W/B_4C	1.3	Small-angle scattering
				28 Å, W/B_4C	1.9	Microbeam fluorescence
						Macromolecular crystallography
G3	W, e^+	y	100%	28 Å, W/B_4C	1.9	*In situ* diffraction/scattering

results of the first test of SiC as a substrate material with a thermal conductivity twice as high as that of Si (§6), followed by a conclusion and future perspectives.

2. Overview of CHESS 'multilayer' beamlines

At present, five out of twelve CHESS beamlines are based on ML optics (Table 1). Some of them (D1, G1 and G3) operate with permanently installed ML monochromators; the others (F3 and A2) alternate their running with silicon optics.

Located in the CHESS East area, hard bending-magnet D1 beamline receives X-rays from the CESR e^+ beam. It was the first CHESS beamline that started regular operation with ML optics. The experimental techniques include small-angle scattering (SAXS), grazing-incidence SAXS (GISAXS), time-resolved radiography and different capillary-based microbeam fluorescence techniques with a variety of samples from such diverse areas as solid-state optoelectronics, environmental studies (plant leaves, fish ear stones *etc.*), archeometry and art heritage. Different coating materials (Mo/B_4C and W/B_4C) and *d*-spacing allow for a wide energy range from 6 keV (fuel spray radiography; MacPhee *et al.*, 2002; Cai *et al.*, 2003) up to 30 keV (archeometry; Powers *et al.*, 2005).

The double-crystal monochromator of the hard bending-magnet F3 beamline (CHESS East, e^+ beam) can accommodate both silicon and ML optics. High-flux MLs with $\Delta E/E = 2.2\%$ are used to study the effect of radiation damage on macromolecular crystals. Recently, this beamline has been used for feasibility studies of using ML optics for protein crystallography (Englich *et al.*, 2005).

The A2 beamline (CHESS West, e^- beam) receives half of the X-ray beam from a 49-pole wiggler. High flux, a wide energy range of up to 60 keV, and flexible design of the monochromator make a variety of experiments possible in diverse areas of material science and solid-state physics. The A2 beamline is operated with ML optics for about half of the beam time. Traditionally, MLs for A2 have been designed to withstand a high-power wiggler beam and produce the highest flux possible (Smolenski *et al.*, 1997, 1998, 2001; Headrick *et al.*, 2002) for time-resolved *in situ* growth of semiconductor thin films (Woll *et al.*, 1999). Recently, MLs with higher energy resolution have been used for *in situ* growth studies of organic thin films (*e.g.* Mayer *et al.*, 2004) which are more susceptible to radiation damage. High-flux MLs are used for imaging experiments, *e.g.* fuel spray radiography with microsecond time resolution.

G-line is a recent addition to CHESS. Two double-crystal ML monochromators deliver wiggler beam to G1 and G3 stations and G2 station receives a small part of the multilayer G3 beam extracted by an X-ray transparent Be crystal. The G1 station was designed for a variety of flux-limited experiments such as SAXS (GISAXS), microbeam fluorescence, and crystallography of small- and medium-unit-cell protein crystals. The G3 station located at the end of the beamline is equipped with a UHV diffractometer for *in situ* growth studies of oxide thin films by pulsed laser deposition (Fleet *et al.*, 2005). The main characteristics and research areas of the CHESS beamlines employing ML optics are summarized in Table 1.

3. High-resolution ML optics

As for crystals, the energy resolution of ML optics is defined by the width of the diffraction curve, $\Delta\theta$, and the Bragg angle θ_B through the simple equation derived from Bragg's law: $\Delta E/E = \Delta\theta \cot\theta_B$. 'Traditional' high-*Z*/low-*Z* MLs (*e.g.* W/C, period $d = 27$ Å, 100 bi-layers, at 10 keV) show a typical first-order reflection width of $\Delta\theta \simeq 0.03^\circ$ and an energy resolution of about 2%. High-resolution MLs are intended to cover the gap between these 'traditional' MLs and silicon optics with $\Delta E/E \simeq 0.01\%$. They can be effectively used in a variety of flux-limited experiments that require better than 1% energy resolution, such as small- and medium-unit-cell size protein crystallography, diffraction from thin films and small crystals, reflectometry, and others. To increase the energy resolution, MLs with much narrower rocking curves are required, and this

can be achieved by increasing the number of layers participating in scattering (Underwood & Barbee, 1981) (in analogy with crystals, by increasing the crystal thickness and thus making the transition from kinematical to dynamical diffraction). The approach, first proposed by Morawe *et al.* (2001*a*,*b*) is based on using a low-contrast (hence, a weak reflectivity at each interface) low-Z (lower absorption and large penetration length), *e.g.* Al_2O_2/B_4C, material combination and increasing the total number of bi-layers to several hundred. Interesting questions arise: What determines the narrowest rocking curve that can be achieved from these artificial periodic structures? Can they compete with crystals? What determines the practical limit?

The Al_2O_2/B_4C MLs with different numbers of bi-layers of up to 800 were made by using magnetron sputtering (for details, see Martynov *et al.*, 2003, 2004; Platonov *et al.*, 2004). Owing to the huge difference in d-spacing between MLs and crystals, the measurement of an 'intrinsic' rocking curve of a high-resolution ML is not trivial because of the dispersion problem. A high-resolution set-up based on two Si(004) channel-cut crystals in an anti-parallel arrangement was used for these purposes at the A2 beamline, as shown in Fig. 1(*a*) (Martynov *et al.*, 2003). Analysis based on DuMond diagrams shows that the angular resolution of this set-up is 4.1 arcsec. In Fig. 1(*b*) the rocking curve of the Al_2O_2/B_4C multilayer with 800 bi-layers and d = 27 Å measured at 10.0 keV is shown with

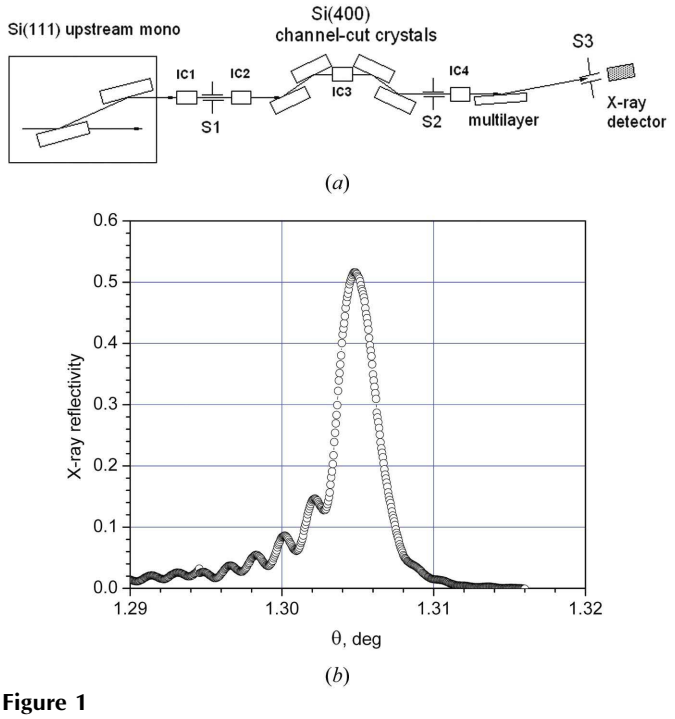

Figure 1
(*a*) High-resolution set-up used at the CHESS A2 wiggler beamline to measure 'intrinsic' reflectivity curves from high-resolution MLs. The Si(111) monochromator defines the energy of the beam and the pair of Si(004) double-bounce channel-cut crystals in a non-dispersive geometry provides 4.1 arcsec angular resolution. Ion chambers IC1–IC4 monitor the beam intensity along the optical path. (*b*) Experimental rocking curve measured from an Al_2O_2/B_4C multilayer with 800 bi-layers and d = 27 Å measured at 10.0 keV. The FWHM (full width at half-maximum) width of the curve is 10.5 arcsec.

Table 2
High-resolution and small d-spacing CHESS multilayers.

N: number of bi-layers. The peak reflectivity is measured at 10.0 keV, and the bandwidth is determined from the FWHM of the rocking curve.

d (Å)	N	Materials	$\Delta E/E$ (%)	Reflectivity (%)	Size (mm)
32	500	Al_2O_3/B_4C	0.3	50	100 × 40 × 30
27	800	Al_2O_3/B_4C	0.22	50	100 × 40 × 30
15	300	W/B_4C	0.5	50	75 × 50 × 5
15	600	Mo/B_4C	0.3	38	75 × 50 × 5
20	300	Mo/B_4C	0.52	65	75 × 50 × 5
22	225	W/B_4C	1.3	75	75 × 50 × 5

a width of only 10.5 arcsec and energy resolution of $\Delta E/E$ = 0.22%. The multilayer structure was deposited on 30 mm-thick Si substrates, thick enough to avoid bending of the substrate by a strained multilayer structure, which would result in the broadening of the rocking curve. The size of the substrate was 100 mm × 40 mm. Remarkably, the width of the rocking curve of these layered synthetic microstructures, 10.5 arcsec, is comparable with the values typical for low-index reflections from perfect crystals [5.6 arcsec for Si(111) and 12.1 arcsec for Ge(111) for 10.0 keV]. The main characteristics of some of the CHESS high-resolution multilayers are shown in Table 2.

The main technological challenge in producing high-resolution low-contrast ML optics is the stability of the deposition equipment over long (typically about 10 h) deposition times. Instabilities and drift of the deposition rate lead to the variations in d-spacing that cause the broadening of the reflectivity curve and deterioration of energy resolution. We concluded that at present the deposition of more than 1500 periods is not practical (Martynov *et al.*, 2003).

ML optics with 0.22% bandwidth, shown in Fig. 1(*b*), have been successfully used at the bending-magnet F3 beamline for protein crystallography experiments using a standard oscillation technique. It was shown (Englich *et al.*, 2005) that the new optics provide a fivefold gain in flux while still allowing the standard equipment and procedures to be used for collecting and processing crystallographic data. We believe that the new optics can be used to collect data from protein crystals with up to 800 Å in unit-cell dimensions, significantly enhancing the capabilities of under-utilized bending-magnet beamlines.

4. Wide-bandpass ML optics

Extending the energy bandpass beyond the typical 2% offered by 'traditional' ML optics opens up new opportunities for a variety of diffraction techniques. In particular, Laue diffraction on macromolecular crystals (Ren & Moffat, 1995) does not require crystal oscillation during exposure, thus presenting the ultimate technique for fast time-resolved crystallography (Bourgeois *et al.*, 2003). Broad reflectivity profiles can be obtained by introducing variations in the ML d-spacing with depth. The idea of depth-graded optics originated from neutron research (*e.g.* Vidal *et al.*, 1992) and was later adopted for X-rays (Erko *et al.*, 1995; Joensen *et al.*, 1997) as an effective way to increase the angle of incidence and, accord-

ingly, reduce the length of an X-ray mirror. At the same time, depth-graded optics extend the energy cut-off while still utilizing the total reflection region for the lower-energy part of the spectra (supermirror concept). Recently, an algorithm to optimize the depth profile and design MLs with specified broad bandwidth was proposed and successfully utilized to produce a ML with 20% bandwidth around 20 keV at a 0.5° incident angle (Morawe *et al.*, 2002). Here, we introduce optics with 5% and 10% bandwidth designed for potential applications in macromolecular crystallography (Platonov *et al.*, 2006).

For their feasibility experiments, CHESS crystallographers requested two pairs of MLs with bandpasses of $\Delta E/E = 5\%$ and 10% with as flat-topped a rocking curve as possible. The *d*-spacing design of depth-graded structures was performed by using a numerical method developed by Protopopov & Kalnov (1998). The method is based on a search algorithm for the best *d*-spacing design through optimization of thickness of each individual layer in the ML structure. Both the 5% and 10% structures contained 100 bi-layers of molybdenum and boron carbide. The thickness of the individual layers varied from 1 nm to 3 nm. The MLs were deposited by the magnetron sputtering technique with the layer thickness controlled by a deposition time. The correlation between the thickness and the deposition time was established during the calibration process, which included deposition of several periodical and depth-graded test structures on flat silicon wafers. The reflectivity curves from the test structures were measured by using a laboratory set-up and Cu $K\alpha$ radiation. Analyzing the reflectivity curves by using a method described by Broadway *et al.* (2004), the layer thickness distribution through the ML stack was reconstructed and compared with the design profile. A few pre-final 5% and 10% structures deposited on silicon wafers were tested at CHESS in the targeted spectral range before performing the final coatings.

Reflectivity curves from two pairs of MLs, measured at the F3 CHESS beamline by scanning the energy of the X-ray beam at a fixed incident angle of 1°, are shown in Fig. 2

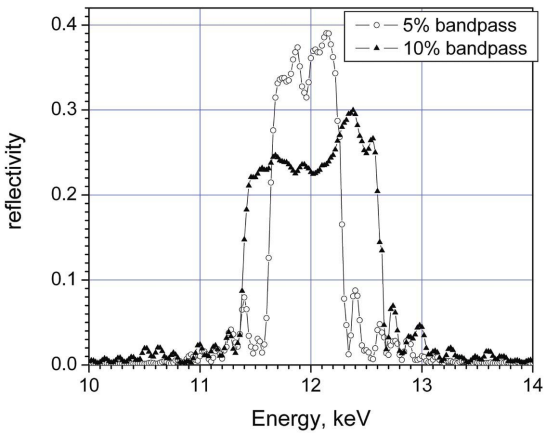

Figure 2
Reflectivity curves from 5% (open circles) and 10% (triangles) broad-bandpass MLs measured by scanning the energy of the upstream Si(111) monochromator at fixed incident angle. MLs were designed to have the energy bandpass centered at 12.0 keV at 1° incident angle.

(Platonov *et al.*, 2006). As one can see, the sides of the energy curves are very sharp, within 100 eV for both 5% and 10% bandpass MLs. The curves in Fig. 2 also confirm the important observation that broad-bandpass MLs cannot be used to increase the integrated photon flux, as the broadening comes at the expense of the maximum reflectivity. Nonetheless, this approach may be effectively utilized in designing X-ray optics with energy bandpass matching characteristics of the synchrotron radiation sources.

5. Small *d*-spacing MLs

Some of the recent CHESS projects based on microbeam fluorescent analysis, such as reading ancient inscriptions (Powers *et al.*, 2005) or studies of art objects (Woll *et al.*, 2005), generated a lot of interest in extending ML optics to 30 keV (Ag, Sn *K*-edges) and higher. The obvious practical limit is the geometrical design constraints of double-crystal monochromators, *i.e.* the minimum vertical and maximum horizontal separation of two crystals. To overcome this problem, MLs with small (<20 Å) *d*-spacing are required. ML technology can reliably produce MLs with a *d*-spacing as low as 15 Å (Platonov *et al.*, 2002; Andreev *et al.*, 2003; Liu *et al.*, 2004). Decreasing *d*-spacing and increasing Bragg angle also implies higher X-ray penetration depth leading to an increased number of layers participating in scattering and a narrower rocking curve. This is the reason why reducing the *d*-spacing is considered as an alternative way to increasing the energy resolution (Martynov *et al.*, 2003). At present, CHESS has MLs available for users with *d*-spacing from 15 Å to 22 Å of two main coatings – W/B_4C and Mo/B_4C. The choice of the coating material for a particular experiment is determined by the energy range: to keep reflectivity high the working energy should be either below or significantly higher than the absorption edge of the composing elements. Experimental reflectivity curves measured by using the high-resolution set-up are shown in Fig. 3 for Mo/B_4C MLs with d = 15 Å and 20 Å. Typical energy resolution values of our small *d*-spacing MLs are in the range 0.3–1%. The defining characteristics (*d*-spacing, material composition *etc.*) of the CHESS small-*d* MLs are listed in Table 2.

Extending the energy range of the ML optics requires detailed knowledge of the energy dependences of their main characteristics. Simulations performed by using the IMD software (Windt, 1998) for the WSi_2/Si MLs with d = 19.7 Å in the energy range from 7 to 25 keV (Liu *et al.*, 2004) show that the reflectivity monotonically increases above the W *L*-absorption edges. Detailed analysis of the main characteristics of ML optics with different *d*-spacing and different material pairs has been performed at CHESS at energies up to 60 keV. The results (CHESS A2 data) for d = 15 Å MLs are shown in Fig. 4 for Mo/B_4C and W/B_4C MLs. As expected, one can see a significant drop in the maximum reflectivity for the Mo/B_4C ML at the Mo *K*-absorption edge at 20.0 keV. At energies above the absorption edge the maximum reflectivity monotonically increases and the width decreases with energy, in agreement with the IMD simulations, as more and more layers

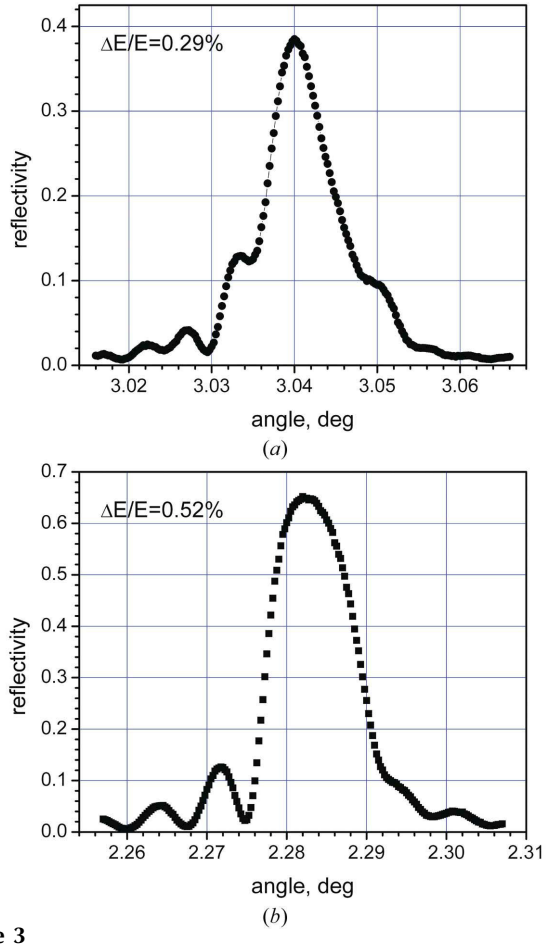

Figure 3
Reflectivity curves measured from small d-spacing MLs at 10.0 keV: (*a*) Mo/B_4C, d = 15 Å, 600 bi-layers; (*b*) Mo/B_4C, d = 20 Å, 300 bi-layers. The energy resolutions of the CHESS small d-spacing MLs are in the range 0.3–1%.

participate in scattering. Some decrease in reflectivity at the highest energy may be attributed to scattering on surface long-range roughness (waviness) at small Bragg angles, which cannot be taken into account by the IMD simulations. As a conclusion based on our experimental results, the ML optics, in fact, show excellent performance at high energy and can effectively replace silicon optics in a variety of flux-limited experiments.

6. ML optics at the CHESS wiggler beamlines

The CHESS West wiggler produces powerful X-ray beams for the A1 and A2 beamlines from the CESR e^- beam and for the G-lines from the e^+ beam. The total X-ray power emitted is 6.6 kW for 200 mA current in the ring. Internally water-cooled MLs have been developed at CHESS (Smolenski *et al.*, 1998) to withstand this wiggler beam and to minimize the thermal bump. They consist of two brazed parts, the bottom part with water channels and water manifold and a flat top part coated with a ML. Internally cooled MLs have been extensively used for many years at the A2 beamline to deliver high flux for *in situ* growth experiments. The typical lifetime of these MLs

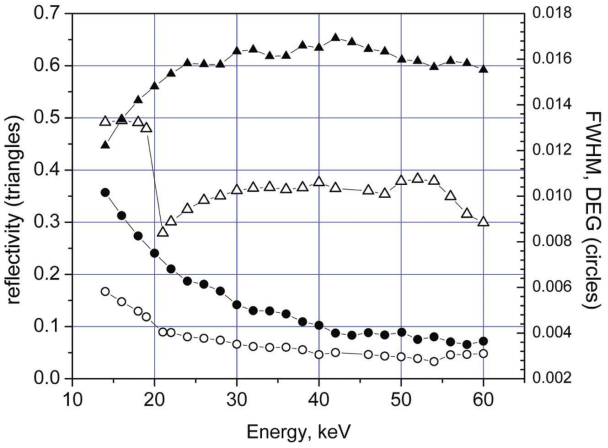

Figure 4
Energy dependences of the reflectivity (left axis, triangles) and the width (right axis, circles) measured from the CHESS small d-spacing MLs: Mo/B_4C, d = 15 Å, 600 bi-layers (open symbols) and W/B_4C, d = 15 Å, 300 bi-layers (solid symbols). A significant drop in reflectivity for the Mo/B_4C multilayer is observed at the Mo K-absorption edge.

spans from a few months to a couple of years of the accumulated beam time. We believe the main factors that contributed to failure are the temperature cycles and severe radiation environment that lead to water leaks and delamination. Installation of a 49-pole wiggler with lower K-value (Finkelstein, 1992) reduced the total power load by 50% but actually increased the power density on the first crystal, and this motivated our search for materials with a higher thermal conductivity than silicon that can be used as substrates for flat contact cooled MLs.

The main constrain in the search for a new potential substrate material is the ability to produce an extremely smooth surface. Until now, the ultimate choice for synchrotron-radiation-based applications was silicon [the material which is commonly used for laboratory sources, fused silica (SiO_2), exhibits extremely low thermal conductivity]. CVD (chemical vapour deposited) silicon carbon attracted our attention owing to a combination of unique properties. It shows a thermal conductivity κ that is twice as high as silicon (300 *versus* 150 $W\,m^{-1}\,K^{-1}$) and slightly lower thermal expansion α that, combined, result in a figure of merit κ/α that is more than twice as high. Other attractive properties of this material include excellent mechanical properties, such as high elastic modulus and toughness, high chemical inertness and radiation resistance. Reaction-bonded SiC, a material with a thermal conductivity that is two times lower than that of CVD SiC, was successfully used recently to produce an internally cooled mirror (Khounsary *et al.*, 2002). The requirements to the surface quality for a high-performance ML is much higher than for an X-ray mirror and, to the best of our knowledge, there are no prior reports about using SiC substrates for ML optics. Here, we present experimental results that unambiguously prove CVD SiC as a perspective material for ML optics with thermal properties superior to Si.

Several identical 25 mm × 75 mm × 5 mm CZ Si and CVD SiC substrates were polished (Wave Precision) to the best effort surface quality. The following average surface figure

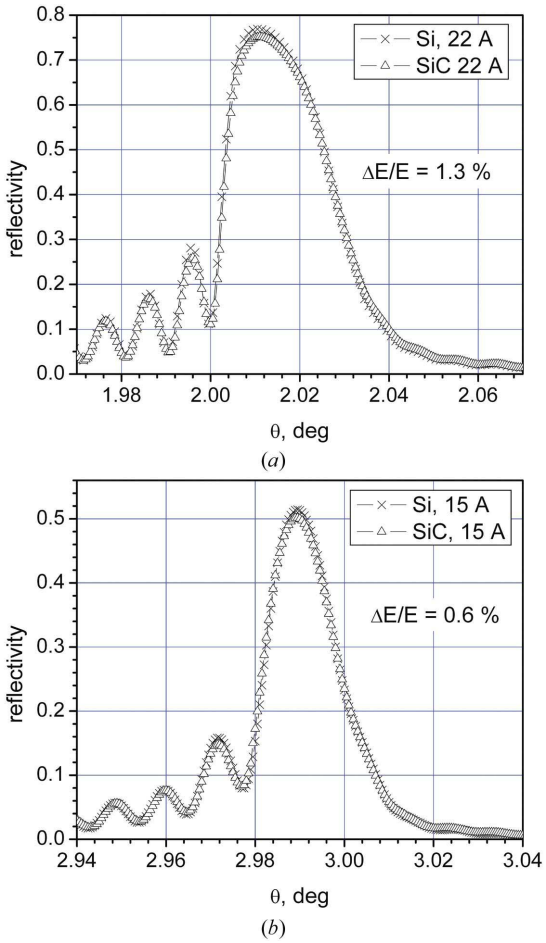

Figure 5
Reflectivity curves from $d = 22$ Å (*a*) and $d = 15$ Å (*b*) W/B_4C multilayers deposited on very smooth and well characterized Si (crosses) and on CVD SiC (triangles) substrates. For each pair of substrates, deposition was performed simultaneously within the same deposition cycle. MLs on SiC substrate show only slightly, ~1%, lower maximum reflectivity.

errors were delivered: RMS roughness of 0.4 Å and 1.1 Å, peak-to-valley roughness of 2.6 Å and 6.8 Å, and slope error of 0.31 arcsec and 0.15 arcsec for Si and SiC, respectively. To achieve high sensitivity to the surface quality, small-period W/B_4C MLs were deposited simultaneously on Si and SiC mirrors with periods of 15 Å (300 bi-layers) and 22 Å (225 bi-layers). Experimental reflectivity curves measured at 10.0 keV by using a high-resolution set-up at the CHESS F3 beamline show almost identical curves with maximum reflectivities of 0.51 and 0.76 for 15 Å and 22 Å MLs (Fig. 5). The maximum reflectivity of the 15 Å ML on SiC is only 1.5% lower than an identical ML deposited on Si.

This experiment proves that excellent quality MLs can be produced on CVD SiC substrates. At present, a typical set of optics for the wiggler A- and G-lines includes a flat ML deposited on a SiC substrate, which is used as a first optical element. The matching flat and fixed-radius sagittal MLs for horizontal focusing are deposited on the Si substrate. All sets are coated with different materials (Mo- and W-based) that are used for different parts of the energy spectrum.

7. Conclusions and outlook

ML optics offer great flexibility in optimizing X-ray flux and energy resolution for a variety of synchrotron radiation experiments. With the availability of many types of MLs – from high-resolution Al_2O_3/B_4C to small *d*-spacing W/B_4C and Mo/B_4C to 'traditional' and, finally, to wide-bandpass optics – the huge energy resolution range from 0.2% to 10% has been successfully covered by CHESS optics. Recent advances in ML technology made possible MLs with rocking-curve widths close to those of perfect crystals. New wide-bandpass ML optics with 5% and 10% bandwidth were designed, tested and introduced for feasibility studies in macromolecular crystallography. Our study of the energy dependencies of the main characteristics of the small *d*-spacing Mo/B_4C and W/B_4C ML optics shows enhancement in their performance at higher energies above absorption edges, making them attractive for use in high-energy flux-limited experiments as an alternative to crystal optics. CVD SiC was introduced as a substrate material with a thermal conductivity that is twice as high as that of Si, and ML optic characteristics comparable with those made on standard high-quality Si substrates. One of our current projects includes studies of MLs with $d < 15$ Å in an attempt to understand what, at the present level of technological development, is the smallest period for which MLs can still offer gain in flux over crystals. Handling heat loads remains a problem. Our experiments show that more than half of the X-ray flux is lost at our wiggler beamlines due to thermal bumps. This problem is even more severe for undulator beams at third-generation sources and future sources such as energy-recovery linacs (Gruner & Bilderback, 2003). Better understanding of the physical mechanisms of heat transfer in a ML structure is required to attack this problem. Finally, coherence preservation is an open question for MLs that has to be answered to assure successful application of ML optics in the fast-growing area of coherent diffraction and imaging.

The support and help of CHESS and MacCHESS staff in testing ML optics and adopting it for a variety of experiments at different CHESS beamlines are greatly acknowledged. This work is based upon research conducted at the Cornell High Energy Synchrotron Source (CHESS) which is supported by the National Science Foundation and the National Institutes of Health/National Institute of General Medical Sciences under NSF award DMR-0225180 and NIH award RR01646.

References

Andreev, S. S., Bibishkin, M. S., Chkhalo, N. I., Kluenkov, E. B., Prokhorov, K. A., Salashchenko, N. N., Zorina, M. V., Schafers, F. & Shmaenok, L. A. (2003). *J. Synchrotron Rad.* **10**, 358–360.
Barbee, T. W. (1981). *AIP Conf. Proc.* **75**, 131–145.
Bilderback, D. H. (1982). *Nucl. Instrum. Methods*, **195**, 67–72.
Bilderback, D. H., Lairson, B. M., Barbee, T. W. Jr, Ice, G. E. & Sparks, C. J. Jr (1983). *Nucl. Instrum. Methods*, **208**, 251–261.
Bourgeois, D., Vallone, B., Schotte, F., Arcovito, A., Miele, A. E., Sciara, G., Wulff, M., Anfinrud, P. & Brunori, M. (2003). *Proc. Natl. Acad. Sci.* **100**, 8704–8709.

Broadway, D. M., Platonov, Y. Y., Martynov, V. V. & Kuo, P. K. (2004). *Proc. SPIE*, **5537**, 133–143.
Cai, W., Powell, C. F., Yue, Y., Narayanan, S., Wang, J., Tate, M. W., Renzi, M. J., Ercan, A., Fontes, E. & Gruner, S. M. (2003). *Appl. Phys. Lett.* **83**, 1671–1673.
Chu, Y. S., Liu, C., Mancini, D. C., De Carlo, F., Macrander, A. T., Lai, B. & Shu, D. (2002). *Rev. Sci. Instrum.* **73**, 1485–1487.
Deschamps, P., Engström, P., Fielder, S., Riekel, C., Wakatsuki, S., Høghøj, P. & Ziegler, E. (1995). *J. Synchotron Rad.* **2**, 124–131.
Englich, U., Kazimirov, A., Shen, Q., Bilderback, D. H., Gruner, S. M. & Hao, Q. (2005). *J. Synchrotron Rad.* **12**, 345–348.
Erko, A., Schaefers, F., Vidal, B., Yakshin, Y., Pietsch, U. & Mahler, W. (1995). *Rev. Sci. Instrum.* **66**, 4845–4846.
Finkelsein, K. D. (1992). *Rev. Sci. Instrum.* **62**, 305–308.
Fleet, A., Dale, D., Suzuki, Y. & Brock, J. D. (2005). *Phys. Rev. Lett.* **94**, 036102.
Gruner, S. M. & Bilderback, D. H. (2003). *Nucl. Instrum. Methods*, A**500**, 25–32.
Haelbach, R.-P. & Kunz, C. (1976). *Opt. Commun.* **17**, 287–292.
Headrick, R. L., Smolenski, K. W., Kazimirov, A., Liu, C. & Macrander, A. T. (2002). *Rev. Sci. Instrum.* **73**, 1476–1479.
Joensen, K. D., Gorenstein, P., Høghøj, P., Susini, J., Ziegler, E., Freund, A., Christensen, F., Wood, J. & Gutman, G. (1997). *Nucl. Instrum. Methods*, B**132**, 221–227.
Khounsary, A. M., Fernandez, P., Assoufid, L., Mills, D., Walters, D., Schwartz, J. & Robichaud, J. (2002). *Rev. Sci. Instrum.* **73**, 1537–1540.
Liu, C., Conley, R., Macrander, A. T., Graber, T. J., Morawe, C., Borel, C. & Dufrense, E. M. (2004). *Proc. SPIE*, **5537**, 154–160.
MacPhee, A. G., Tate, M. W., Powell, C. F., Yue, Y., Renzi, M. J., Ercan, A., Narayanan, S., Fontes, E., Walther, J., Schaller, J., Gruner, S. M. & Wang, J. (2002). *Science*, **295**, 1261–1263.
Martynov, V. V., Platonov, Yu., Kazmirov, A. & Bilderback, D. H. (2003). *Proc. SPIE*, **5195**, 46–53.
Martynov, V. V., Platonov, Yu., Kazmirov, A. & Bilderback, D. H. (2004). *AIP Conf. Proc.* **705**, 697–700.
Mayer, A. C., Ruiz, R., Headrick, R. L., Kazimirov, A. & Malliaras, G. (2004). *Org. Electron.* **5**, 257.
Morawe, C., Peffen, J.-C., Ziegler, E. & Freund, A. K. (2001*a*). *Proc. SPIE*, **4145**, 61–71.
Morawe, C., Peffen, J.-C., Ziegler, E. & Freund, A. K. (2001*b*). *Proc. SPIE*, **4501**, 127–134.
Morawe, C., Ziegler, E., Peffen, J.-C. & Kozhevnikov, I. V. (2002). *Nucl. Instrum. Methods*, A**49**, 189–198.
Pennartz, P. U., Löchner, U. & Fuess, H. (1992). *J. Appl. Cryst.* **25**, 571–577.
Platonov, Y., Broadway, D., Kazimirov, A. & Xiao, X. (2006). In preparation.
Platonov, Yu., Gomez, L. & Broadway, D. (2002). *Proc. SPIE*, **4782**, 152–159.
Platonov, Yu., Martynov, V., Kazimirov, A. & Lai, B. (2004). *Proc. SPIE*, **5537**, 161–170.
Powers, J., Dimitrova, N., Huang, R., Smilgies, D.-M., Bilderback, D. H., Clinton, K. & Thorne, R. E. (2005). *Z. Papyrol. Epigr.* **152**, 221–227.
Protopopov, V. V. & Kalnov, V. A. (1998). *Opt. Commun.* **158**, 127–140.
Ren, Z. & Moffat, K. (1995). *J. Appl. Cryst.* **28**, 461–481.
Smolenski, K. W., Headrick, R. L., Liu, C. & Macrander, A. T. (2001). *Proc. SPIE*, **4145**, 22–27.
Smolenski, K. W., Headrick, R. L., Shen, Q., Carroll, B., Khounsary, A. M., Liu, C. & Macrander, A. T. (1998). *Proc. SPIE*, **3448**, 27–31.
Smolenski, K. W., Shen, Q. & Doing, P. (1997). *AIP Conf. Proc.* **417**, 66–70.
Stephenson, G. B. (1988). *Nucl. Instrum. Methods*, A**266**, 447–451.
Underwood, J. H. & Barbee, T. W. Jr (1981). *Appl. Opt.* **20**, 3027–3034.
Underwood, J. H., Thimpson, A. C., Wu, Y. & Giauque, R. D. (1988). *Nucl. Instrum. Methods*, A**266**, 296–302.
Vidal, B., Jiang, Z. & Samuel, J. (1992). *Proc. SPIE*, **1738**, 30–41.
Windt, D. L. (1998). *Comput. Phys.* **12**, 360–370.
Woll, A. R., Bilderback, D. H., Gruner, S., Gao, N., Huang, R., Bisulca, C. & Mass, J. (2005). *Proc. Mater. Res. Soc.* **852**, 002.5.
Woll, A. R., Headrick, R. L., Kycia, S. & Brock, J. D. (1999). *Phys. Rev. Lett.* **83**, 4349–4352.
Ziegler, E., Marot, G., Freund, A. K., Joksch, St., Kawata, H., Berman, L. E. & Iarocci, M. (1992). *Rev. Sci. Instrum.* **63**, 496–499.